Available online at www.sciencedirect.com
SCIENCE DIRECT
Earth and Planetary Science Letters 244 (2006) 501–514
EPSL
www.elsevier.com/locate/epsl

Magnetic study of an Antarctic weathering profile on basalt: Implications for recent weathering on Mars

V. Chevrier [a,*], P.-E. Mathé [b], P. Rochette [b], H.P. Gunnlaugsson [c]

[a] Arkansas Center for Space and Planetary Sciences, 202 Old Museum Building, University of Arkansas, Fayetteville, AR 72701, USA
[b] CEREGE, Europôle Méditerranéen de l'Arbois, BP80, 13545 Aix-en-Provence Cedex 04, France
[c] The Mars Simulation Laboratory, Ny Munkegade, Bldg. 520, University of Aarhus, DK-8000 Aarhus C, Denmark

Received 26 July 2005; received in revised form 5 January 2006; accepted 20 February 2006
Available online 29 March 2006
Editor: V. Courtillot

Abstract

In order to better interpret the Martian surface weathering-related mineralogy, we focused on a relevant analogue of the Martian subsurface in terms of lithology and paleoclimate: the Jurassic-aged Ferrar dolerite (Priestley Glacier, Transantarctic Mountains), weathered in cold and dry climate. Together with chemical and mineralogical studies, rock magnetic properties were investigated and completed with Mössbauer measurements. Weathering of the decimetric block is evidenced by chemical profiles showing an increase in Fe content (from 10.5 in the core to 13 wt.% in the surface) and a decrease in Si (from 57 to 53 wt.%, respectively). According to mineralogical, thermomagnetic and hysteresis properties, the main opaque mineral is inherited titanomaghemite, with a concentration about 1%. Enhancement in low field magnetic susceptibility (from $4 \cdot 10^{-6}$ to $10 \cdot 10^{-6}$ m^3/kg, respectively) and saturation magnetization (from 0.44 to 0.96 Am^2/kg, respectively) indicates the neoformation of metastable maghemite. Neoformed red ferric (oxy)hydroxides are abundant in the surface. High field susceptibility normalized to iron concentration and Mössbauer spectra indicate a replacement of Fe^{2+} from primary silicates (pyroxene) by poorly crystalline antiferromagnetic Fe^{3+} (oxy) hydroxides. Thus, highly magnetic titanomaghemite and maghemite coexist with nanosized ferric (oxy)hydroxides and primary silicates, in accordance with Martian in situ observations. Therefore, this study supports the formation of the Martian regolith as resulting from a slow weathering process in near present day conditions.

Keywords: Antarctica; Ferrar dolerite; Mars; regolith; rock magnetism; weathering

1. Introduction

The surface of Mars is globally covered by an oxidized regolith made of fine dust particles mixed with basaltic sands and rocks. However, the mechanisms behind the origin of this altered regolith are poorly understood. Spectroscopic observations from orbiters and landers showed the abundance of ferric iron (oxy) hydroxides in the Martian regolith [1], resulting probably from alteration of mafic to ultramafic primary material [2]. Various phases may describe the spectroscopic properties including nanophase red hematite [3], goethite [4], ferrihydrite [5] and iron-rich clays [6,7]. Recent Mössbauer analyses performed by Mars

* Corresponding author. Tel.: +1 479 575 3170.
E-mail addresses: vchevrie@uark.edu, chevrier@cerege.fr (V. Chevrier).

0012-821X/$ - see front matter © 2006 Elsevier B.V. All rights reserved.
doi:10.1016/j.epsl.2006.02.033

Exploration Rovers (MER) indicate the presence of abundant paramagnetic and poorly crystalline (oxy) hydroxides in the Martian regolith [8]. Finally, magnetic experiments onboard Viking, Mars Pathfinder and MER evidenced 1% to 7% of a strongly magnetic phase which nature is currently not precisely known [9], but which magnetization is about 5 Am^2/kg [10].

Various mechanisms may explain such coexistence of strongly colored and magnetic iron phase(s), including palagonitisation by hydrothermal or surface liquid water [11], weathering through interaction with volcanic acidic products [12] and atmosphere-induced meteoric weathering [13]. Terrestrial red soils developed on basaltic rocks usually show a strong magnetic signal carried by primary spinel inherited during weathering of parent rock [14,15]. Secondary maghemite can form also during soil formation [16]. Most studied terrestrial red soils have formed under tropical climate, which is far away from the present day (and probably back to 4 Gy) arid and cold climate on the surface of Mars. This difference in (paleo)climate between Mars and Earth may have an important influence on the weathering kinetics of primary phases as well as on the nature and crystallinity of the alteration products. Metastable phases, which are rapidly converted into stable minerals in a warm and wet climate, could be preserved in colder conditions and become the dominant weathering products [17]. Some authors have highlighted the importance of metastable phases in the alteration products of basalt in cold and dry climate [18].

Antarctic samples have been extensively studied to test their relevance to Martian surface. Various studies focused on sediments as analogues of potential paleo-lakes on Mars, searching for mineralogical and chemical biomarkers [19]. A few studies on weathering of basaltic material have been conducted, particularly on the mineralogical changes and physicochemical processes [20]. These studies demonstrated the formation of clays and iron (oxy)hydroxides as resulting from weathering by thin layers of liquid water. However, no extensive study of an Antarctic weathering profile has yet been published, from the point of view of the mineralogical and magnetic properties. In the present study, we focus on the Antarctic Ferrar Dolerite as an analogue for the basaltic Martian crust [21]. This mid-Jurassic andesitic basalt (~180 My) widely outcrops in the Victoria Land as sills, dikes and lava flows intruded in the Beacon sandstones and the underlying basement complex [22]. The use of Ferrar dolerite as a relevant analogue of Martian surface is based first on the dry and cold climate reigning in Antarctica, and also on petrology. Indeed, space orbiter observations reveal a basaltic to andesitic composition of the Martian surface lithosphere [23]. This surface petrology is quite similar to the Ferrar dolerite, which is a fine-grained tholeiitic to andesitic basalt, composed of pyroxenes, plagioclases with small amounts of Fe–Ti oxides and scarce pyrrhotite [22].

2. Methods

2.1. Sample description and preparation

The profile used from our study comes from an unoriented decimetric block of Ferrar dolerite, collected by A. Meloni during a PNRA (Programma Nazionale di Ricerche in Antartide-Italian National Research Program in Antarctica) expedition near the Priestley Glacier, Antarctica (163°E, 74°S, 3000 m of altitude). At this altitude, air temperature never exceeds −10 °C, so that the presence of liquid water is limited to the rare moments when sun radiations heating the dark rock surface are sufficient to create a liquid film at the contact between the rock and surrounding snow. The bloc has an irregular shape, and is completely covered by a brown layer (Fig. 1), comparable to varnishes usually observed

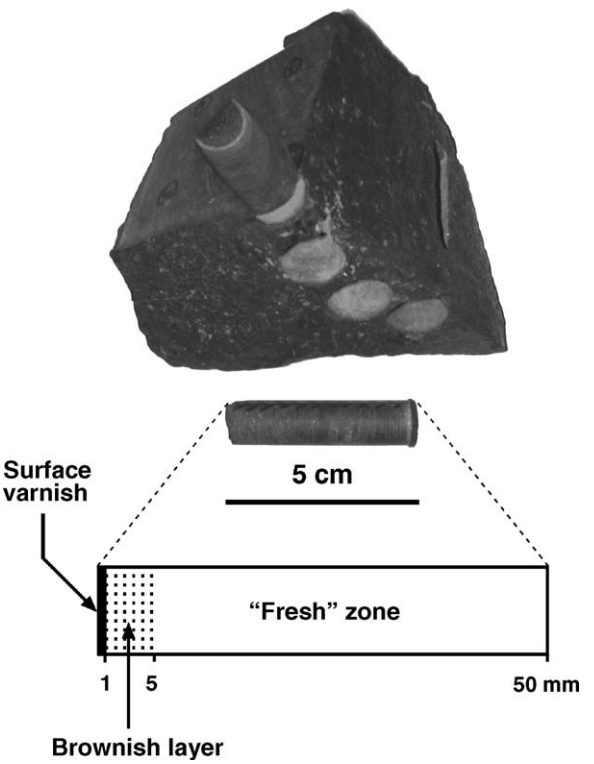

Fig. 1. Photograph of the Ferrar dolerite sample showing the weathered crust. A drill core used for magnetic characterizations is presented, as well as a schema of the apparent structure of the weathering profile.

on rocks weathered in Antarctica [24]. The brown layer has an almost constant thickness of about 1 mm and is prolonged by a slightly discoloured zone observable down to 5 mm in the profile. There is no visible discontinuity between the surface layers and underlying rock. In order to investigate magnetic properties and chemical profiles, some cores were drilled along the weathering gradient, perpendicularly to the obviously most weathered surface (main diameter of the block: 7 cm). The cores, 4 to 5 cm length for a diameter of 8 mm (Fig. 1), were then subsampled into 1.5 mm thick slices using a high precision diamond wire saw. We obtained approximately 25 slices weighting about 0.5 g each. We have converted thickness of slices into depth along the weathering profile. Finally, the uppermost superficial fraction (about 0.5 mm thick layer) has been manually sampled using a Dremel abrasion tool.

2.2. Rock magnetic properties

Slices have been used for the characterization of low field magnetic susceptibility χ_{LF} and hysteresis parameters (coercive field B_C, remanent coercive force B_{CR}, saturation magnetization M_S and remanent magnetization M_{RS}) along the weathering profile. Bulk χ_{LF} measurements have been done using an AGICO Kappabridge KLY2, with noise level less than $5 \cdot 10^{-9}$ m^3/kg. The KLY2 was coupled with a CS2 probe for χ_{LF} versus temperature curves, in the range 20–600 °C, on about 1 g of ground rock. χ_{LF} versus temperature curves have been done both in air and under an argon flow. Finally, hysteresis and remanence measurements were realized on a P.M.C. VSM micromagnetometer Model 3900. Hysteresis cycles were done on each slice (i.e. about 0.5 g of rock) with a 1 T maximum field and a step of 10 mT. Noise level in high field is about $5 \cdot 10^{-4}$ Am^2/kg and tends to 10^{-5} Am^2/kg in low field. Hysteresis parameters (B_C, M_S and M_{RS}) were determined after a slope correction applied at high field (800 mT), from which is derived the high field susceptibility χ_{HF}.

^{57}Fe transmission Mössbauer spectra (TMS) of fresh core and weathered surface were measured at room temperature using conventional constant acceleration drive systems and 10–50 mCi ^{57}Co:Rh sources [25]. The velocity scale was calibrated using the magnetic sextuplet spectrum of a high purity iron foil absorber and the origin of isomer shift scale was determined from the centre of the α-Fe spectrum. The absorber thickness was in the range 3–5 mg/cm^2. Conversion electron Mössbauer spectra (CEMS) were recorded by placing the sample on a double adhesive conducting tape as the cathode in a parallel plate avalanche detector.

2.3. Petrologic, mineralogical study and chemical analyses

To complete magnetic analyses, we carried out observations in transmitted and reflected light on a thin section made along the weathering profile. SEM observations and EDX (energy dispersive X-ray) analyses of oxides, (oxy)hydroxides and sulfides were carried out on the same thin section, using a JEOL JSM-6320F (CRMCN, University of Aix-Marseille III, Luminy, Marseille) with an accelerating tension of 15 kV (Fig. 3a,b,e). Some additional SEM photographs of the thin section and the surface of the rock (Fig. 3f,g, h) were taken using a Philips XL 30 ESEM (environmental scanning electron microscope) with an accelerating tension of 20 kV. We also performed bulk chemical analyses on the thin slices used for magnetic measurements, using an ICP-AES spectrometer and the following protocol: about 0.3 g of material is finely ground in an agate mortar and heated at 900 °C in a graphite crucible to obtain the loss on ignition (LOI). The material is fused in $LiBO_2$ and then dissolved in HCl, for injection in the spectrometer line.

3. Experimental results

The 33 mm depth slice, corresponding to the geometric centre of the block, was chosen as the least weathered sample and thus as a reference to compute relative changes in percent for all chemical and magnetic parameters along the weathering profile (Tables 1 and 2), using the formula:

$$X_{Z,33} = \frac{X_Z - X_{33}}{X_{33}} \times 100. \quad (1)$$

3.1. Chemical and mineralogical properties

3.1.1. Bulk chemical analyses

Bulk chemical analyses show evolution of elements concentrations in the first 5 mm (Table 1, Fig. 2), characterized by a relative decrease/increase in specific elements, compared to the deeper fresh zone, which values are nearly constant [26]. The most affected mobile element is Si, which content decreases from about 57 wt.% SiO_2 in the fresh zone to 53 wt.% at the surface. Immobile elements Fe and Mn increase in the first 5 mm from 10.6 wt.% to 13 wt.% Fe_2O_3 and from 0.2 wt.% to 0.27 wt.% MnO (Table 1). Strongly

Table 1
Chemical concentrations of main elements used for weathering characterization

Depth (mm)	Na_2O	MgO	Al_2O_3	SiO_2	K_2O	CaO	TiO_2	MnO	FeO	H_2O (110 °C)	LOI [a]	Zr (ppm)
33 [b]	2.01	4.39	13.31	56.96	1.37	8.79	1.00	0.20	10.51	0.31	0.98	142
29	7.79	−1.24	−0.48	−0.04	6.87	−2.61	4.81	−1.24	−0.18	31.68	2.88	8.45
25	10.62	4.07	5.28	−3.72	7.93	3.27	1.71	2.60	3.88	43.32	1.79	7.75
21	6.45	0.04	0.62	0.17	1.65	−1.78	−3.01	−2.01	−0.49	17.59	−14.26	3.52
17	12.90	−1.84	0.37	−0.30	12.13	−5.05	0.87	−6.09	2.02	44.98	−13.51	15.49
13	15.99	0.07	−1.46	−0.71	19.59	−2.92	−0.07	−6.03	1.32	58.27	3.04	9.86
9	1.53	4.42	2.41	−2.09	3.90	−1.04	−6.95	−6.85	5.66	30.73	10.31	15.49
5	11.44	−1.28	2.57	−2.84	24.68	−1.85	0.11	−12.58	4.77	29.52	33.56	22.54
3	15.93	0.57	7.98	−7.15	31.27	0.68	−0.83	2.05	14.06	94.37	45.78	28.17
1	8.25	−3.76	0.75	−7.16	27.76	−5.69	−1.18	32.06	24.39	108.69	120.11	33.80

[a] Loss on ignition: volatiles lost when heating the sample at 900 °C for the ICP-AES—corresponds mainly to bonded water.
[b] The first line represents 33 mm reference values. All the other concentrations are expressed in percent relative to the 33 mm value, using the formula given in the text.

immobile elements Ti and Zr show different behaviour: while Zr increases continuously from the core (150 ppm) to the surface (190 ppm), Ti presents a constant concentration of 1 wt.%. Ti and Zr are generally used as indicator of porosity generated by dissolution of primary silicates and glass [26]. Based on the Zr profile, this should indicate a mass loss of about 25% in the surface and thus a porosity of 25% assuming no change of the volume (i.e. compression or dilatation). This value is unrealistic when considering observations of thin sections (see below). Moreover, if the increase in Zr was due to porosity then Ti should follow the same trend. An alternative explanation for this differential behaviour may be the remobilization of Zr along the weathering profile. Even if Zr and Ti are considered to be strongly immobile, some studies have evidenced that these elements can be mobile at a local scale depending on the phases in which they are concentrated [27]. This may indicate that Zr is concentrated in the glass, a phase highly sensitive to weathering, whereas Ti is mainly present in the Fe–Ti oxides, which are more resistant, as evidenced in the following sections. Finally, H_2O lost at 110 °C as well as LOI (loss on ignition: volatiles lost when heating at

Table 2
Magnetic parameters

Depth (mm)	χ_{LF}	χ_{HF}	M_S (Am^2/kg)	M_{RS} (Am^2/kg)	M_{RS}/M_S	B_C	B_{CR}	B_{CR}/B_C
33 [a]	4268 $10^{-9}m^3/kg$	159.1 $10^{-9}m^3/kg$	0.44 Am^2/kg	0.10 Am^2/kg	–	11.1 mT	21.1 mT	–
33	0.0	0.0	0.0	0.0	0.223	0.0	0.0	1.90
31	1.9	−1.8	2.9	4.1	0.221	1.2	0.8	1.89
29	5.7	0.2	5.3	3.8	0.216	0.0	0.4	1.94
27	12.0	0.3	12.2	8.1	0.227	−1.8	−0.1	1.87
25	16.2	−0.9	14.3	6.2	0.220	−5.0	−1.7	1.87
23	26.1	−2.6	21.4	9.0	0.202	−9.1	−4.1	1.97
21	38.8	0.0	34.2	16.9	0.196	−10.9	−4.9	2.00
19	45.7	0.1	41.7	21.6	0.196	−12.1	−6.1	2.01
17	63.1	0.9	60.0	38.1	0.197	−10.5	−5.8	2.01
15	71.6	−1.4	70.2	46.5	0.196	−10.0	−4.9	2.04
13	80.1	0.2	78.8	53.6	0.199	−10.0	−5.6	2.03
11	86.3	0.4	89.7	67.8	0.205	−7.5	−4.6	2.01
9	76.9	1.8	91.2	84.7	0.212	2.1	0.0	1.97
7	87.5	−0.8	103.8	102.7	0.220	5.3	3.5	1.94
5	115.2	−4.1	115.9	104.1	0.225	−3.8	−1.9	1.91
3	126.5	−0.3	111.1	104.7	0.231	−4.8	−5.8	1.90
1	135.8	7.7	118.7	114.0	0.228	−5.6	−5.9	1.91

Abbreviations: χ_{LF}: low field susceptibility, χ_{HF}: high field susceptibility, M_S: saturation magnetization, M_{RS}: saturation remanent magnetization, B_C: coercive field, B_{CR}: remanent coercive force.
[a] The first line represents 33 mm reference values, all the other being expressed in percent relative to 33 mm using the formula given in the text, except for M_{RS}/M_S and B_{CR}/B_C ratios for which rough values are given.

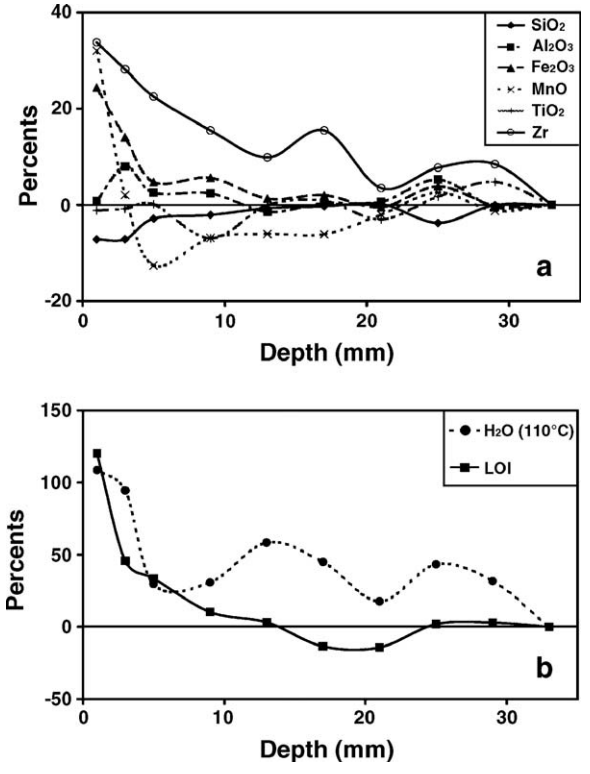

Fig. 2. Evolution with depth of the main elements concentrations relative to the concentration measured at 33 mm. See text for the formula.

high temperature) indicate a doubling of free and bounded water content, mostly in the first 5 mm (Table 1, Fig. 2). Note that non hydrated phases–e.g. carbonates, sulfates, sulfides or organics–may also contribute to the LOI. This 5 mm thick layer, in which chemical depletion occurs, corresponds exactly to the brownish layer observed on thin section.

3.1.2. Observations with microscope and SEM

Phases observed in reflected light are mainly Fe–Ti oxides, exhibiting prismatic to acicular habits (Fig. 3a) with a size below $40 \times 5\,\mu m$. SEM observations and EDX analyses of oxides show different phases present in crystals (Fig. 3a), corresponding to different Ti content: ilmenite ($FeTiO_3$–Fe/Ti ≈ 1), Ti-rich spinel (Fe/Ti = 3.6) and Fe-rich spinel (Fe/Ti = 8.5 or $x = 0.3$ in the general formula of titanomagnetite: $Fe_{3-x}Ti_xO_4$). The Fe-rich spinel of main formula $Fe_{2.7}Ti_{0.3}O_4$ is the most frequently observed. No difference in Fe/Ti ratio of spinel has been noticed between the fresh core and the weathered surface. Oxidation state (or z parameter) of spinel has not been determined as it requires measurement of oxygen content, which was impossible to carry out with this instrument.

Ferrar dolerite contains also scarce sulfides, generally less than 1 μm sized and exceptionally reaching 10 μm. Sulfide is mainly pyrrhotite as evidenced by reflected light and SEM (Fig. 3b) observations as well as EDX analyses. The pyrrhotite is present in the fresh core zone but disappears near the surface, and some of the pyrrhotite grains are weathered with iron (oxy)hydroxides filling cleavage planes and fractures (Fig. 3b). Sulfates have not been observed but are probably mixed with (oxy)hydroxides resulting from pyrrhotite weathering.

Observations of Ferrar dolerite in transmitted light show the presence of (oxy)hydroxides replacing pyroxene crystals along cracks or cleavage planes and filling vugs (Figs. 3c and d). (Oxy)hydroxides are also filling some small veins (thickness <0.5 mm) across the rock and often linked to the surface (Fig. 3e). These veinlets are responsible for heterogeneities in chemical profiles and magnetic properties. (Oxy) hydroxides are abundant near the surface, present in all pyroxene grains and scarcer in the fresh core, only in a few pyroxene grains. (Oxy)hydroxides exhibit plasma structures or concentric accumulations (Figs. 3d and e) without any visible crystal, even with the highest magnification (×1000).

Near the surface, small areas, typically hundred of micrometers sized, show very slight development of porosity (Fig. 3f). In these zones, the negative print of primary dissolved minerals leaves in relief phases like spinel (Fig. 3f). In the same zones, scarce grains of Ti-free Fe spinel (Fig. 3g) have been detected. As these grains are associated to porous zones, they could have formed during weathering. Finally, SEM observations show that the surface of the rock is covered by a few tens of micrometers thick varnish composed of clay minerals (Fig. 3h), evidenced by qualitative chemistry (Si, Al, K, Na, Fe elements) as well as foliated structure. EDX analyses indicate abundant NaCl crystals are also present on the surface (Fig. 3h), embedded in clays which protect them from dissolution. The presence of NaCl crystals results probably from trapping of marine aerosols, due to the proximity of the Antarctic Ocean, and confirms that liquid water, when present in the sample, was lost only by evaporation or freezing plus sublimation.

3.2. Magnetic properties

3.2.1. Low field magnetic susceptibility χ_{LF} and thermomagnetic properties

χ_{LF} increases continuously along the weathering profile (Fig. 4), extending from $4.3 \cdot 10^{-6}\,m^3/kg$ in the

core to $10 \cdot 10^{-6}\,m^3/kg$ in the surface, which represents an increase of 136% compared to the 33 mm core value (Table 2). Using the chemical composition determined by EDX analyses, χ_{LF} values correspond to an averaged spinel content of about 1% in the Ferrar dolerite, which is in good accordance with textural observations on

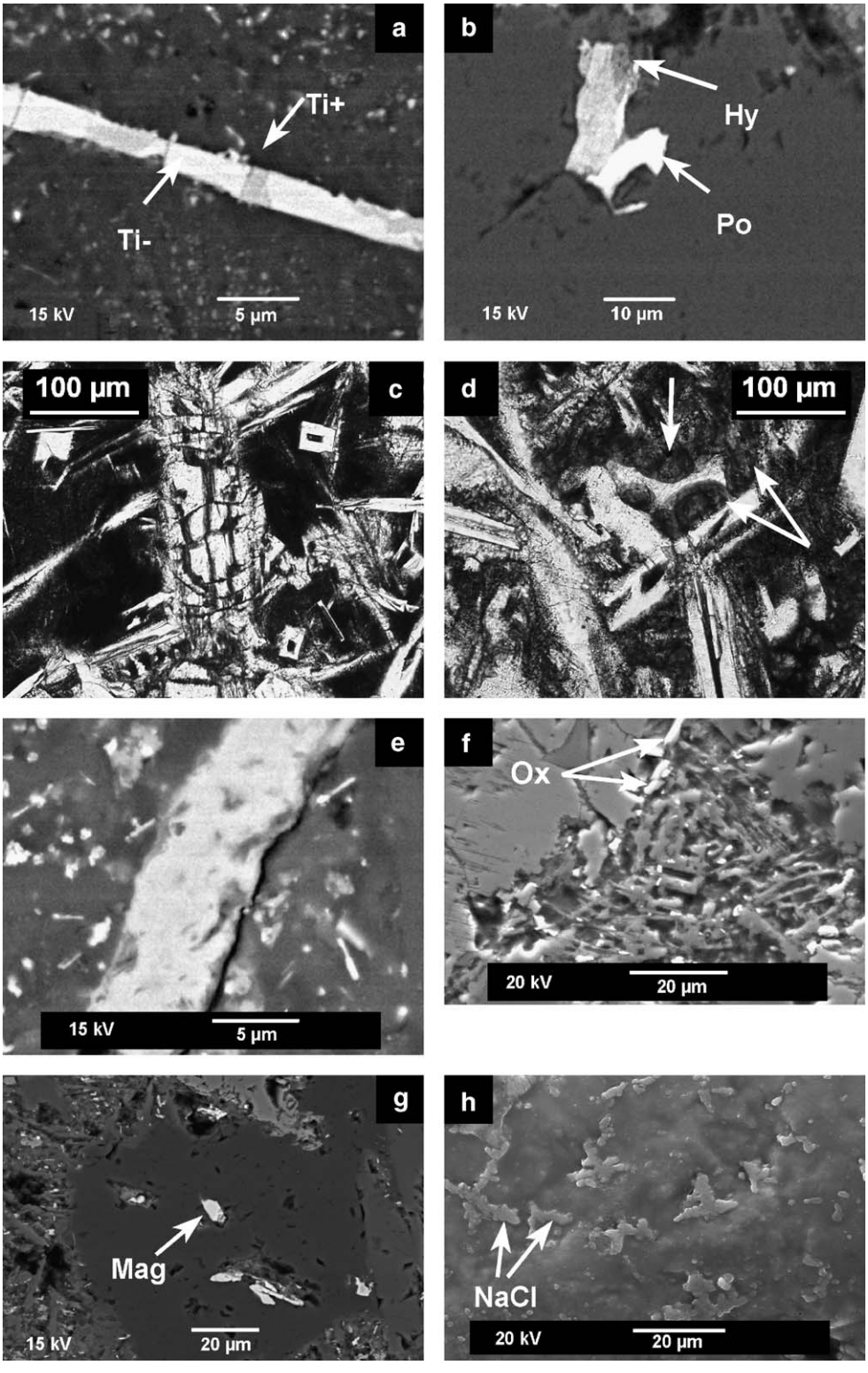

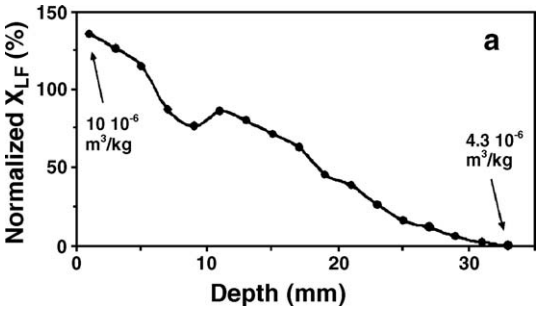

Fig. 4. (a) Low field magnetic susceptibility χ_{LF} (expressed in percent relative to the value of the 33 mm deep slice) versus depth. Absolute values of the first and last slice are also indicated on the figure.

polished section. Using different values of χ_{LF} [28], the highest spinel content does not exceed 5% in the surface. χ_{LF} versus temperature curves of the fresh core are very similar in air and in argon, characterizing low-Ti substituted spinel (Fig. 5), with a Curie temperature in the range 560–580 °C. Previous work identified low-Ti titanomagnetite as the main magnetic carrier in Ferrar dolerite [29]. Nevertheless, the presence of a decrease between 400 °C and 450 °C in both heating curves (Fig. 5) followed by an increase in χ_{LF} between 450 °C and 500 °C is typical of titanomaghemite inversion [30,31]. This titanomaghemite corresponds to the Fe–Ti spinel observed with SEM. Despite the similar behaviour of titanomaghemite upon heating, there is a weak difference between surface and core signals, with a slight inflection point around 350 °C only observed in the heating curve of the surface sample (Fig. 5). This feature indicates small amount of γ-Fe_2O_3 maghemite.

The surface layer sample (thickness <0.5 mm) presents completely different signal compared to the rest of the rock (Fig. 5). Heating curve in air is typical of maghemite with an inversion in hematite beginning between 300 and 400 °C, and completed at 620 °C. The heating curve in argon shows a Curie temperature of 570 °C indicating magnetite formation from reduction of maghemite. The cooling curve gives a Curie temperature of 580 °C and a much higher χ_{LF}, confirming formation of magnetite upon heating. Moreover, the maghemite inversion after 300 °C in argon indicates that it is pre-existing in the rock and not formed during the heating in oxidizing air. Therefore, on the base of χ_{LF} versus temperature curves, the magnetic profile is composed of a mixture between two phases: maghemite evidenced in the surface layer, which results probably from neoformation, and primary titanomaghemite. No signal related to iron (oxy)hydroxides can be detected in thermomagnetic curves, due to overwhelming spinel signal [28].

Fig. 6 presents χ_{LF} measured at room temperature after heating at various temperatures under an argon flow, characterizing irreversible mineralogical transformations. The curve of the fresh core shows a continuous increase between 25 and 500 °C followed by a drop between 500 and 600 °C, with χ_{LF} loss about 20%. This drop corresponds to titanomaghemite inversion. This inversion signal is also present in the curve of the weathered surface but up to 700 °C, indicating that titanomaghemite is more oxidized, and thus release more titanohematite upon heating. The surface signal shows also a decrease between 300 and 450 °C, which disappears progressively towards the fresh core. This feature corresponds to the inversion of maghemite into hematite, resulting in a diminution of χ_{LF}. These results confirm the formation of nearly pure maghemite superposed to the contribution of primary titanomaghemite. At lower temperatures, curves of fresh core and weathered surface show a small jump between 210 and 240 °C likely to correspond to relaxation of stress in magnetic grains. Moreover, this increase is higher for the surface, where the stress linked to oxidation of grains is more important.

3.2.2. High field magnetic susceptibility χ_{HF}

High field susceptibility χ_{HF} characterizes paramagnetic Fe^{2+} silicates and antiferromagnetic/paramagnetic Fe^{3+} (oxy)hydroxides, supposing that all spinel phases have reached saturation. χ_{HF} appears constant within ±5% from the 33 mm value of $159 \cdot 10^{-9}$ m^3/kg, except

Fig. 3. Microphotographs and SEM pictures of Ferrar dolerite. All pictures are taken from the thin section except for the picture F corresponding to the sample weathered surface. (a) SEM picture of primary oxide (titanomaghemite) showing white Ti-poor zones (Ti−) and grey Ti-rich zones (Ti +). (b) SEM picture of Primary pyrrhotite (Po) showing a beginning of weathering with formation of (oxy)hydroxides (Hy). (c) Microphotograph in transmitted light: detailed picture showing a pyroxene crystal filled with neoformed (oxy)hydroxides along cleavage planes and fractures. (d) Microphotograph in transmitted light: detailed picture showing the colloidal structure of neoformed (oxy)hydroxides (arrows). (e) SEM picture of small vein filled with neoformed (oxy)hydroxides showing a plasma structure. (f) SEM picture of grains of magnetite/maghemite (Mag) completely deprived of titanium embedded in porous glass (dark grey) surrounded by silicates showing a stronger porosity. This picture has been taken in the weathered zone, near the surface. (g) SEM picture of a porous zone showing the negative prints of weathered primary minerals and the remaining white oxides (Ox) appearing in relief. (h) SEM picture of the surface layer showing NaCl crystals embedded in a clay phase covering the entire sample surface.

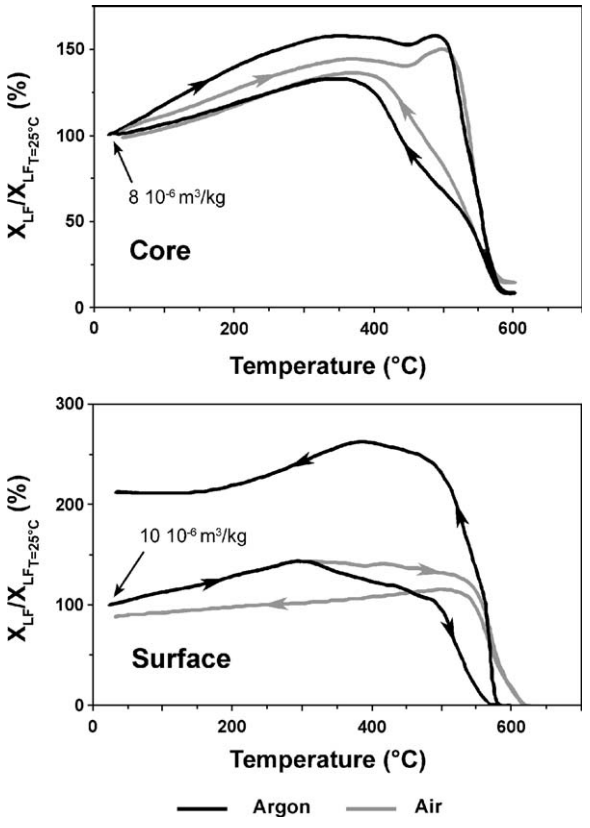

Fig. 5. χ_{LF} versus temperature in air and in argon of core and surface layer (first 500 μm of the surface—see Fig. 1). Values are expressed in percents of room temperature value.

the surface sample where it increases by 8%. We use the following formula [32] to determine the iron percentages corresponding to the χ_{HF} values:

$$\chi_{HF} = -5 + 25.2t_{Fe^{2+}} + 33.4t_{Fe^{3+}} \text{ in } 10^{-9} \text{ m}^3/\text{kg} \quad (2)$$

with t_x corresponding to atomic weight percentages of elements in the rock. The first value in the formula is the diamagnetic susceptibility of quartz taken as an approximation for all diamagnetic minerals. We suppose here that all the other paramagnetic elements (Mn, Cu, Co, Ni, etc.) are negligible against Fe (MnO content under 0.5 wt.%). Application of this formula to the fresh core gives a paramagnetic iron content in the 4.9–6.5 wt.% range, for Fe^{3+} or Fe^{2+}, respectively. This is consistently lower than the measured Fe content (i.e. 8.2% Fe in the core). Although the presence of spinel can account for 1–2 wt.% of this missing iron, antiferromagnetically ordered Fe^{3+}-bearing phases have to be invoked to explain the too low χ_{HF} signal (see further evidence from Mössbauer data).

3.2.3. Hysteresis properties

Saturation magnetization (M_S) and saturation remanent magnetization (M_{RS}) signals are dominated by the spinel. Both profiles show a continuous increase from the core to the surface of the block (Fig. 7a) with M_S and M_{RS} values ranging from 0.44 Am^2/kg to 0.96 Am^2/kg and from 0.1 Am^2/kg to 0.21 Am^2/kg, respectively. The corresponding relative increases of respectively 114% and 118% are in good agreement with the χ_{LF} profile. Taking an average M_S value of 60 Am^2/kg for titanomaghemite ($x=0.3$) and maghemite [28], the spinel content ranges from 0.7% in the core to 1.6% in the surface, in agreement with values obtained using χ_{LF}. Coercive force B_C and remanent coercive force B_{CR} profiles are also very similar, although more complex than the other profiles (Fig. 7b). Between 33 mm and 19 mm, B_C and B_{CR} profiles show a decrease of 12% and 5%, respectively. From 21 mm to 13 mm, both profiles are relatively flat. From 13 mm to the surface, B_C and B_{CR} increase up to a maximum at 7 mm deep, where B_C reaches 11.7 mT and B_{CR} 21.9 mT before decreasing again. This complex behaviour of coercive force can be interpreted in term of evolution of grain size and oxidation degree.

B_{CR}/B_C and M_{RS}/M_S evolution along weathering profiles (Fig. 7c) are also suitable parameters to get constraints on oxidation state and grain size. Both profiles show exactly opposite behaviour with increasing B_{CR}/B_C and decreasing M_{RS}/M_S from 33 mm to 20 mm indicating an increase either in grain size [33,34] or in oxidation degree [35]. According to the χ_{LF} profile, the weathering gradient affects also the core (cf. maghemite formation). Therefore, both results indicate rather partial oxidation of primary titanomaghemite. This oxidation induces also the concomitant diminution

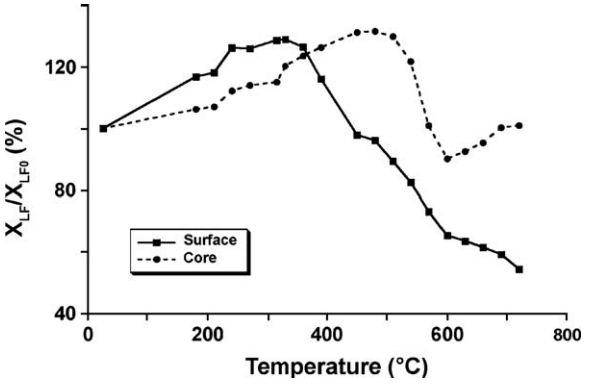

Fig. 6. Measurement of χ_{LF} at 25 °C of surface and fresh core samples, after heating at various temperatures. Values are expressed in percents of initial room temperature value, i.e. $2.6 \cdot 10^{-3}$ Am^2/kg for the core and $4.8 \cdot 10^{-3}$ Am^2/kg for the surface sample.

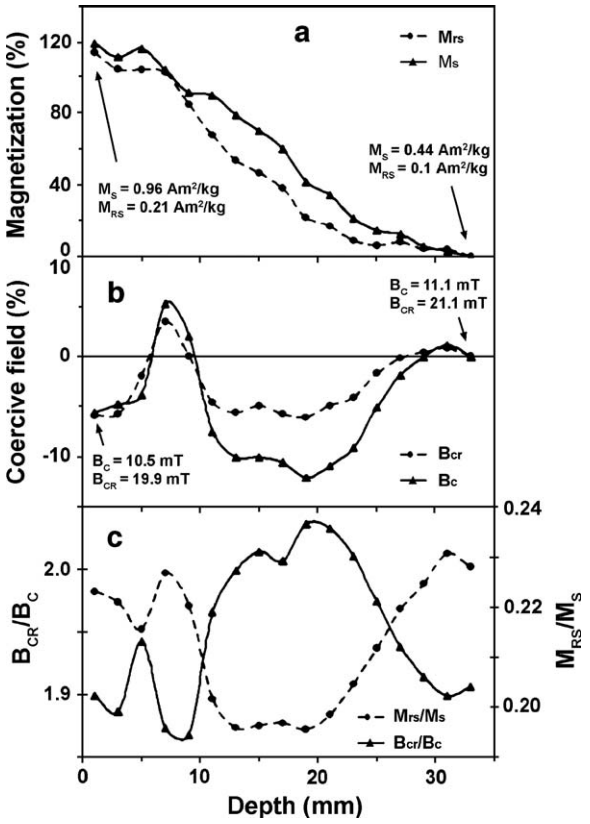

Fig. 7. Hysteresis parameters versus depth (absolute values of the first and last slice are indicated on the figure for magnetizations and coercitive forces): (a) saturation magnetization (M_S) and remanent saturation magnetization (M_{RS}), expressed in percents relative to the 33 mm slice. (b) Coercive force (B_C) and remanent coercive force (B_{CR}), expressed in percents relative to the 33 mm slice. (c) M_{RS}/M_S and B_{CR}/B_C ratios.

of B_{CR} and B_C. From 13 mm to 7 mm deep, B_{CR}/B_C decreases, while M_{RS}/M_S increases. As a diminution of oxidation degree is unrealistic in this zone, this feature likely corresponds to formation of maghemite, as evidenced by χ_{LF} profile and χ_{LF} versus temperature curves. Thus, the variations of B_{CR}/B_C and M_{RS}/M_S result from maghemite small grain size as increasing concentration induces a diminution of average grain size of spinel in the rock. This interpretation is also confirmed by coercive forces (B_C and B_{CR}) increases towards the surface. Consequently, the whole hysteresis properties result from the superposition of two profiles resulting from weathering: the first one corresponds to the slight oxidation of primary titanomaghemite, and the second to formation of maghemite. Thus, the relatively flat profiles between 21 mm and 13 mm result probably from the superposition of titanomaghemite oxidation and maghemite formation. Finally, from 7 mm deep to the surface, the decrease in M_{RS}/M_S and increase in B_{CR}/B_C may be due either to the transformation of maghemite into hematite or to the dissolution of the smallest grains of titanomaghemite. The decrease of coercive forces B_C and B_{CR} seems to argue rather for the dissolution effect, even in the arid environment prevailing in Antarctica. Hysteresis properties have been further investigated by first order reversal curves (FORC) diagrams. The analysis of these FORC diagrams confirms the above interpretation without bringing important extra information. Therefore, we present these diagrams as online material without detailed interpretation.

3.2.4. Magnetic parameters normalized to iron content

Magnetic mineralogy changes may be better characterized from magnetic parameters normalized to iron concentrations. Fe-normalized M_S (Fig. 8a) and χ_{LF} (Fig. 8b) present very similar profiles. The deep part of

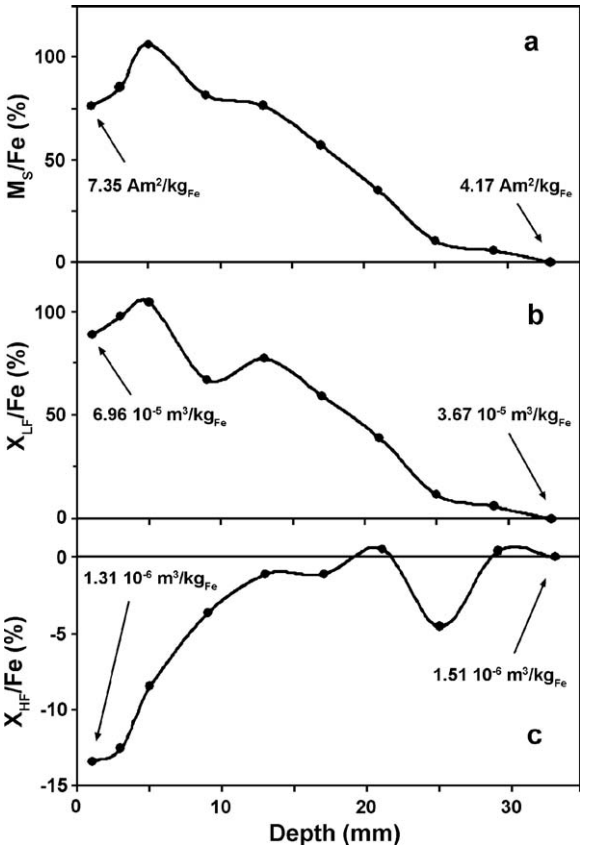

Fig. 8. Magnetic parameters normalised to iron content (expressed in percents relative to the 33 mm slice) versus depth. These parameters are used to characterize mineralogical evolutions along the weathering gradient. Absolute values of the first and last slice are also indicated on the figure for each parameter: (a) saturation magnetization M_S, (b) low field susceptibility χ_{LF}, (c) high field susceptibility χ_{HF}.

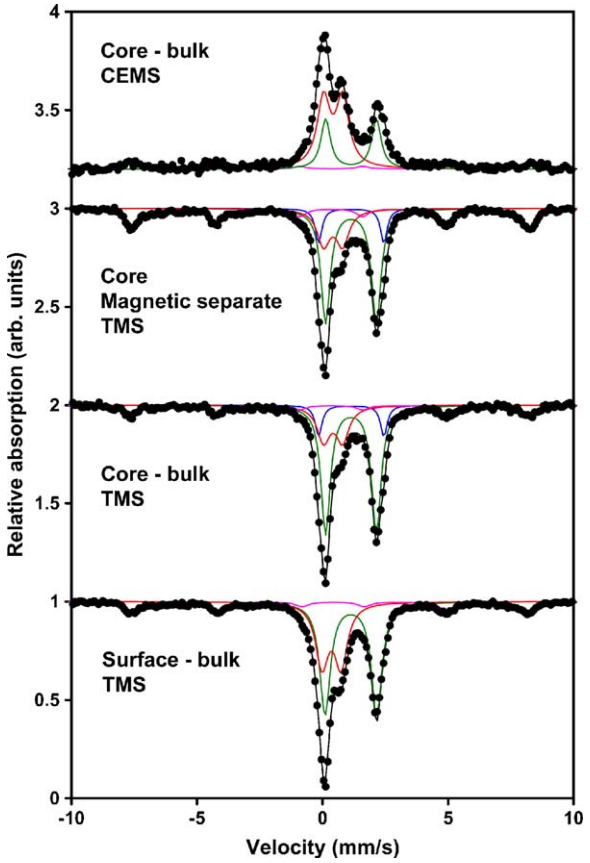

Fig. 9. Mössbauer spectra of fresh core and weathered surface recorded at room temperature (TMS: transmission Mössbauer spectroscopy, CEMS: conversion electron Mössbauer spectroscopy). Full lines represent extrapolated subspectra and their sum (green: paramagnetic Fe^{2+}-M1 site in pyroxene, blue: paramagnetic Fe^{2+}-M2 site in pyroxene, red: paramagnetic Fe^{3+}, purple: magnetically ordered ferric oxide, black: sum of the various components). (For interpretation of the references to colour in this figure legend, the reader is referred to the web version of this article.)

the profile, up to 25 mm, is relatively flat, indicating a nearly constant mineralogy attributed to titanomaghemite. Between 25 and 13 mm, both profiles show a strong increase of about 75%, due to neoformed maghemite. Near the surface, after 5 mm, Fe-normalized M_S and χ_{LF} show a slight decrease due to the transformation of maghemite into hematite/ferric (oxy) hydroxides as evidenced by hysteresis parameters. This corresponds also to the brownish zone, where Fe^{3+} (oxy)hydroxides are abundant. The Fe-normalized χ_{HF} profile (Fig. 8c) is used to evidence the presence of (oxy)hydroxides. Indeed, the profile is relatively flat up to 10 mm indicating a constant mineralogy, due to paramagnetic Fe^{2+} and Fe^{3+} in pyroxenes, with the exception of a drop around 25 mm. After 10 mm, the normalized χ_{HF} profile shows a progressive decrease, indicating the replacement of paramagnetic Fe^{2+} in pyroxenes by antiferromagnetic Fe^{3+} in (oxy)hydroxides [36]. Finally, in the most superficial part of the profile, after 3 mm, the flat profile indicates relative accumulation of Fe^{3+} through silicate dissolution, as confirmed by the loss of Si (Table 1). The local heterogeneity of χ_{HF} at 25 mm is due to a veinlet of (oxy)hydroxides across the slice (Fig. 3e). This hypothesis is corroborated by chemical analyses, and particularly the Si abundance, showing a drop at the same depth, while Fe increases slightly (Table 1).

3.3. Mössbauer spectroscopy

^{57}Fe TMS (transmission Mössbauer spectroscopy) results are summarized in Fig. 9 and Table 3. The spectra of each sample were analysed simultaneously. This means that one assumes that the spectra of different separates/measurements are analysed with the assumption that the spectra contain the same spectral

Table 3
Mössbauer parameters obtained from a simultaneous analysis of core and surface samples of Ferrar dolerite

Core sample Mössbauer parameter	Fe^{2+}, M1	Fe^{2+}, M2	Fe^{3+}	Ferric oxide
B_{hf} (T)				48.96(7)
δ (mm/s)	1.136(3)	1.145(5)	0.422(7)	0.333(9)
ΔE_Q (mm/s)	2.02(2)	2.60(3)	0.75(2)	−0.03(2)
Γ (mm/s)	0.45(2)	0.32(4)	0.62(2)	0.68(4)
				0.59(5)
A_b (%)	54(3)	9(2)	20.6(9)	15(2)
A_m (%)	46(3)	9(2)	19.2(8)	24(2)
A_{CEMS} (%)	26(3)	11(2)	50(2)	11(2)

Surface sample Mössbauer parameter	Fe^{2+}	Fe^{3+}	Ferric oxide
B_{hf} (T)			48.5(2)
δ (mm/s)	1.130(4)	0.359(7)	0.36(2)
ΔE_Q (mm/s)	2.056(7)	0.76(2)	−0.14(4)
Γ (mm/s)	0.510(9)	0.61(2)	0.81(9)
			0.64(10)
A_b (%)	50(2)	33.4(8)	16(2)

The numbers in the parenthesis are the 1σ errors in the last digit. B_{hf}: magnetic hyperfine field, δ: isomer shift, ΔE_Q: quadrupole splitting (doublets) or quadrupole shift (=2ε, sextet), Γ: Lorentzian width, in the case of sextet, only the Γ_{16} and Γ_{34} are given, Γ_{25} is assumed to be the average, A: relative spectral area (b: bulk, m: magnetic separate, CEMS: reflexion spectrometry).
Mössbauer parameters: Fe^{2+}: Fe^{2+} in pyroxene with two different crystallographic sites used in the case of the core sample: M1 and M2, Fe^{3+}: paramagnetic Fe^{3+} component, ferric oxide: magnetically coupled ferric iron oxide (see text for details).

components in different amounts. This method gives more reliable analysis of the spectra, better error estimates and allows one to make conclusions on small spectral features, which is more difficult in the analysis of individual spectra. The Fe^{3+} component in the core sample was rather small to be determined with any accuracy, so CEMS (conversion electron Mössbauer spectroscopy) measurement was performed to complete analysis. Here, it is only applied as a technical method to determine the parameters of the components, as CEMS spectra enhance more highly oxidized features in the spectra [10]. A measurement on a magnetic separate of the core sample was also performed, to better characterize highly magnetic phases. Spectra of the same samples were analysed by assuming the same spectral components with varying intensity. In the case of the core sample, four spectral components were used, including the Fe^{2+} component in the pyroxene, with two different octahedral crystallographic sites M1 and M2, a paramagnetic Fe^{3+} component and a magnetically ordered ferric oxide. The parameters of the doublets are in good agreement with the assignments. The relatively high isomershift of the Fe^{3+} component is more consistent with Fe^{3+} in pyroxene (δ usually larger than 0.4 mm/s) than secondary oxidation products (δ usually less than 0.4 mm/s) [25]. The ferric oxide has very broad lines, but as there is no reason to expect that this is more than one phase (no significant change in parameters in the magnetic separate), it is consistent with a phase characterized by distribution in Fe environments, i.e. a Fe–Ti spinel. The quadrupole shift suggests titanomaghemite rather than titanohematite. The difference between data and experimental fit shows a six-line pattern, with the outermost lines at about −6.4 mm/s and 7.5 mm/s indicating the presence of a component with considerable Fe^{2+} character. Such difference is characteristic for not fully oxidized titanomaghemite [37]. The signal is too small to be included in the analysis, but could represent 1–2% of the bulk spectrum. From these results and the iron content, the ferric oxide has saturation magnetization about 20 Am^2/kg, which is consistent with titanomaghemite, although significantly lower than the value determined from the Ti content (60 Am^2/kg).

Contrarily to the core sample, it was very difficult in the measurement of the surface sample to identify clearly the M1 and M2 crystallographic sites, so the fit was done with a single component (Fe^{2+}). The results obtained by using the parameters determined from the core sample analysis were practically identical. The determination of the ferric oxide is not as accurate, though the parameters suggest more of a hematite nature. The difference between the spectrum and the fit shows similar differences as in the core sample, but less pronounced. Moreover, there must have been a formation of almost pure maghemite to account for the high saturation magnetization of the sample. The Fe^{3+} component has here lower isomershift, consistent with secondary iron (oxy)hydroxides (i.e. not Fe^{3+} in pyroxene).

4. Discussion

4.1. The magnetic phase in the Martian regolith

In addition to magnetic experiments, complementary Mössbauer analyses have been carried to better constrain the nature of the magnetic phase(s) on Mars. MER Spirit evidenced on the surface of Martian rocks the presence of non-stoichiometric magnetite, resulting from partial oxidation of Fe^{2+} into Fe^{3+} and/or Ti substitution [8], whereas spectra of the dust collected on the magnets showed rather magnetite [38]. Alternatively, composite particles of maghemite and iron (oxy) hydroxydes or silicates have been mentioned to explain the strong difference of saturation magnetization between pure maghemite (M_S = 60–65 Am^2/kg) and Martian fines [39]. Several pathways may explain its presence, including transformation from parent phases like lepidocrocite [6,40] or ferrihydrite [27,41] and precipitation from solutions [42]. Moreover, superparamagnetic nanocrystalline hematite [3], feroxyhyte [43] or even partially altered elemental iron [13] may conciliate magnetic and spectroscopic data.

The present study shows that terrestrial basalt weathering under very cold and arid climate presents mineralogical similarities with tropical laterites [27,44], with highly magnetic fraction inherited from parent bedrock associated to colored ferric (oxy)hydroxides. χ_{LF} versus temperature analyses and Mössbauer spectra identify unambiguously titanomaghemite along the weathering profile, in agreement with Spirit's Mössbauer spectrum of Adirondack rock surface in Gusev Crater. The presence of titanomaghemite rather than titanomagnetite may result from deuteritic alteration occurring at the end of the emplacement of the basalt [27,45], explaining the strong similarity of titanomaghemite between the surface and the core of the Ferrar dolerite sample. Therefore, due to its high stability, the titanomaghemite is conserved through weathering [44] and is then probably a major magnetic phase in the Martian regolith [15].

When taking titanomaghemite as a possible candidate to account for the strongly magnetic phase in the Martian regolith, it is important to consider that its

saturation magnetization is strongly dependent on its Ti content [28,33]. All Martian SNC meteorites, and especially the shergottites, show Ti-rich spinel [46]. Therefore, the main carrier of magnetization in the majority of SNC meteorites is pyrrhotite rather than titanomagnetite [47]. However, for an averaged Ti-content, different spinel phases often crystallize depending on the various and complex exsolutions phenomena during cooling history of the host rock. The Ferrar dolerite presents various spinel compositions ranging from high- ($x=0.7$) to low-Ti ($x=0.3$) content, the Ti-poor spinel M_S being about five times higher [28]. Even when considering a high Ti content of primary rock, a highly magnetic primary spinel may crystallize or be exsolved.

In addition to titanomaghemite, secondary maghemite resulting from pyroxene weathering could represent an important component of the highly magnetic phase [48]. Maghemite could account for a part of the oxidized phase(s) identified in Mössbauer spectra of Martian rocks and dust [8,38]. Then, weathering of basaltic rocks in cold and dry climate provides an efficient and simple pathway to the formation of maghemite through weathering in conditions similar to today's cold and dry Martian environment. Nevertheless, our study suggests that maghemite is metastable with respect to hematite. This character has been evidenced in other studies of maghemite formation [40,41]. Therefore, the conservation of maghemite along the profile may result from slower transformation kinetics induced by cold temperatures, whereas higher temperatures should rather favour hematite [49,50]. Thus, the detection of maghemite on Mars may indicate that weathering is still efficient today on Mars. Furthermore, composite particles of maghemite and hematite mixture may describe the lower saturation magnetization of the observed magnetic phase on Mars [38,39]. We have also observed the presence of a thin layer of clays on the surface of the Ferrar dolerite. Therefore, formation of clays in current Martian conditions is possible even if extremely limited, as requiring the presence of liquid water. In addition, clays may be associated to maghemite/titanomaghemite as the composite particles observed on Mars [39].

4.2. Iron (oxy)hydroxides on Mars

In the Ferrar dolerite, ferric (oxy)hydroxides are resulting mainly from pyroxene weathering and accumulate near the surface of the rock. High field magnetic characterizations, Mössbauer spectroscopy and structures suggest nanophase, paramagnetic and poorly crystalline ferric (oxy)hydroxides. Similar increases of poorly crystalline paramagnetic ferric (oxy)hydroxides have also been evidenced on the surface of rocks and in the soil in Gusev Crater [8], suggesting that weathering may be still active in the cold and dry Martian environment [6]. Rates are much slower considering lower temperature and water activity, as evidenced by other Antarctic studies [51] but the mechanism remains similar [26]. Weathering in Antarctica and on Mars may occur through interaction with liquid water films resulting from atmospheric condensation, ice melting and brine films [20]. Therefore, hydrated minerals in the Martian regolith are probably an important reservoir of bonded and adsorbed water [52]. According to chemical profiles of Ferrar dolerite, up to 2.5 wt.% free and bonded water in neoformed phases accumulate near the surface of the sample, a content very similar to the Martian regolith, as measured by Viking Landers (2% water, linked to iron (oxy)hydroxides or hydrated sulfates [53]) or APXS (Alpha Proton X-ray Spectrometer) onboard Mars Pathfinder [54]. Thus, a part of the water in the Martian regolith should be linked to poorly crystalline ferric (oxy)hydroxides and clays.

The important hypothesis for making Ferrar dolerite an appropriate analogue of Martian surface is the similarity between Martian and Antarctic climates considering water and temperatures. Using cosmogenic in situ produced elements, maximum exposure ages of Dry Valley rock have been determined to be as high as 10 Ma [55]. Other studies demonstrate a glacial-polar climate reigning in Antarctica since the Miocene [56] with mean temperatures well below 0 °C. Thus, Ferrar dolerite is likely to have been weathered in a constant polar type climate, at least since the last 10 My. This duration may appear very short if compared to the 3 Gy of nearly constant climate on Mars. Nevertheless, it indicates also that, if the dolerite has been weathered in only 10 My, then the Martian surface must also have undergone substantial weathering, even in conditions of lower water partial pressure.

5. Conclusions

Through this extensive study of a weathering profile developed on the Ferrar dolerite, we have evidenced strongly magnetic spinels, i.e. titanomaghemite inherited from primary rock and secondary maghemite, associated to poorly crystalline ferric (oxy)hydroxides. These phases are relevant to Martian in situ magnetic experiments and Mössbauer observations and suggest an obvious analogy between weathering processes of Martian and Antarctic basalts. A terrestrial type

pedogenetic process in cold and dry climate, still active today, may be responsible for an important part of the regolith properties, without involving features absent today, i.e. abundant liquid water (rain and surface flow), hydrothermalism etc. Weathering occurs through temporary interaction of the rock surface with condensed water from atmosphere and/or ice melting. Recent weathering may also explain the contradictory presence in the regolith of primary (olivine) and highly altered material. According to this study, relatively unaltered primary pyroxenes coexist with secondary iron (oxy) hydroxides in the uppermost part of the profile. Further eolian erosion of these surfaces may lead to the coexistence of both primary and secondary materials in the soil, but also on the surface of the rocks.

Appendix A. Supplementary figure

Supplementary figure associated with this article can be found, in the online version, at doi:10.1016/j.epsl.2006.02.033.

References

[1] J.F. Bell III, H.Y. McSween Jr., J.A. Crisp, R.V. Morris, S.L. Murchie, N.T. Bridges, J.R. Johnson, D.T. Britt, M.P. Golombek, H.J. Moore, A. Ghosh, J.L. Bishop, R.C. Anderson, J. Brückner, T. Economou, J.P. Greenwood, H.P. Gunnlaugsson, R.M. Hargraves, S. Hviid, J.M. Knudsen, M.B. Madsen, R. Reid, R. Rieder, L. Soderblom, Mineralogic and compositional properties of Martian soil and dust: results from Mars Pathfinder, Journal of Geophysical Research 105 (E1) (2000) 1721–1755.

[2] J.F. Mustard, S. Erard, J.-P. Bibring, J.W. Head, S. Hurtrez, Y. Langevin, C.M. Pieters, C.J. Sotin, The surface of Syrtis Major: composition of the volcanic substrate and mixing with altered dust and soil, Journal of Geophysical Research 98 (E2) (1993) 3387–3400.

[3] R.V. Morris, D.G. Agresti, H.V. Lauer Jr., J.A. Newcomb, T.D. Shelfer, A.V. Murali, Evidence for pigmentary hematite on Mars based on optical, magnetic, and Mössbauer studies of superparamagnetic (nanocrystalline) hematite, Journal of Geophysical Research 94 (B3) (1989) 2760–2778.

[4] R.V. Morris, D.C. Golden, Goldenrod pigments and the occurrence of hematite and possibly goethite in the Olympus-Amazonis Region of Mars, Icarus 134 (1) (1998) 1–10.

[5] J.L. Bishop, H. Fröschl, R.L. Mancinelli, Alteration processes in volcanic soils and identification of exobiologically important weathering products on Mars using remote sensing, Journal of Geophysical Research 103 (E13) (1998) 31457–31476.

[6] A. Banin, T. Ben-Schlomo, L. Margulies, D.F. Blake, L. Mancinelli, E.U. Gehring, The nanophase iron mineral(s) in Mars soil, Journal of Geophysical Research 98 (E11) (1993) 20831–20853.

[7] J.L. Bishop, C.M. Pieters, R.G. Burns, J.O. Edwards, R.L. Mancinelli, H. Fröschl, Reflectance spectroscopy of ferric sulfate-bearing montmorillonites as Mars soil analog materials, Icarus 117 (1995) 101–119.

[8] R.V. Morris, G. Klingelhöfer, B. Bernhardt, C. Schröder, D.S. Rodionov, P.A. de Souza Jr., A. Yen, R. Gellert, E.N. Evlanov, J. Foh, E. Kankeleit, P. Gütlich, D.W. Ming, F. Renz, T. Wdowiak, S.W. Squyres, R.E. Arvidson, Mineralogy at Gusev Crater from the Mössbauer spectrometer on the Spirit Rover, Science 305 (5685) (2004) 833–836.

[9] M.B. Madsen, P. Bertelsen, W. Goetz, C.S. Binau, M. Olsen, F. Folkmann, H.P. Gunnlaugsson, K.M. Kinch, J.M. Knudsen, J. Merrison, P. Nornberg, S.W. Squyres, A.S. Yen, J.D. Rademacher, S. Gorevan, T. Myrick, P. Bartlett, Magnetic properties experiments on the Mars Exploration Rover mission, Journal of Geophysical Research 108 (E12) (2003) #8069.

[10] H.P. Gunnlaugsson, Analysis of the magnetic properties experiment data on Mars: results from Mars Pathfinder, Planetary and Space Science 48 (2000) 1491–1504.

[11] H.E. Newsom, J.J. Hagerty, F. Goff, Mixed hydrothermal fluids and the origin of the Martian soil, Journal of Geophysical Research 104 (E4) (1999) 8717–8728.

[12] A. Banin, F.X. Han, A. Cicelsky, Aciditic volatiles and the Mars soil, Journal of Geophysical Research 102 (E6) (1997) 13341–13356.

[13] V. Chevrier, P. Rochette, P.-E. Mathé, O. Grauby, Weathering of iron rich phases in simulated Martian atmospheres, Geology 32 (12) (2004) 1033–1036.

[14] P.-E. Mathé, P. Rochette, F. Colin, The origin of magnetic susceptibility and its anisotropy in some weathered profiles, Physics and Chemistry of the Earth 22 (1–2) (1997) 183–187.

[15] J.M.D. Coey, S. Morup, M.B. Madsen, J.M. Knudsen, Titanomaghemite in magnetic soils on Earth and Mars, Journal of Geophysical Research 95 (B9) (1990) 14423–14425.

[16] A.T. Goulart, J.D. Fabris, M.F.d.J. Filho, J.M.D. Coey, G.M.d. Costa, E.D. Grave, Iron oxides in a soil developed from basalt, Clays and Clay Minerals 46 (4) (1998) 369–378.

[17] R.B. Singer, Spectral evidence for the mineralogy of high-albedo soils and dust on Mars, Journal of Geophysical Research 87 (B12) (1982) 10159–10168.

[18] C. BenderKoch, S. Morup, M.B. Madsen, L. Vistisen, Iron-containing products of basalt in a cold-dry climate, Chemical Geology 122 (1995) 109–119.

[19] J.L. Bishop, B.L. Anglen, L.M. Pratt, H.G.M. Edwards, D.J. Des Marais, P.T. Doran, A spectroscopy and isotope study of sediments from the Antarctic Dry Valleys as analogs for potential paleolakes on Mars, International Journal of Astrobiology 2 (2003) 273–287.

[20] W.W. Dickinson, M.R. Rosen, Antarctic permafrost: an analogue for water and diagenetic minerals on Mars, Geology 31 (3) (2003) 199–202.

[21] C.C. Allen, J.L. Conga, Weathering of basaltic rocks under cold, arid conditions: Antarctica and Mars (abstract), Proceedings of Lunar and Planetary Science 21 (1991) 711–717.

[22] B.M. Gunn, Differentiation in Ferrar dolerites, Antarctica, New Zealand Journal of Geology and Geophysics 5 (1962) 820–863.

[23] J.L. Bandfield, V.E. Hamitlon, P.R. Christensen, A global view of Martian surface compositions from MGS-TES, Science 287 (2000) 1626–1630.

[24] G.P. Glasby, J.G. McPherson, B.P. Kohn, J.H. Johnston, J.R. Keys, A.G. Freeman, M.J. Tricker, Desert varnish in southern Victoria Land, Antarctica, New Zealand Journal of Geology and Geophysics 24 (1981) 389–397.

[25] N.N. Greenwood, T.C. Gibb, Mössbauer Spectroscopy, Chapman and Hall, London, 1971.

[26] R.A. Eggleton, C. Foudoulis, D. Varkevisser, Weathering of basalt: changes in rock chemistry and mineralogy, Clays and Clay Minerals 35 (1987) 161–169.
[27] P.-E. Mathé, P. Rochette, D. Vandamme, F. Colin, Volumetric changes in weathered profiles: iso-element mass balance method questioned by magnetic fabric, Earth and Planetary Science Letters 167 (1999) 255–267.
[28] C.P. Hunt, B.M. Moscowitz, S.K. Banerjee, Magnetic properties of rocks and minerals, Rock Physics and Phase Relations, A Handbook of Physical Constants, American Geophysical Union, Minneapolis, 1995, pp. 189–204.
[29] R. Lanza, E. Zanella, Paleomagnetism of the Ferrar dolerite in the northern Prince Albert Mountains (Victoria Land, Antarctica), Geophysical Journal International 114 (1993) 501–511.
[30] Ö. Özdemir, Inversion of titanomaghemites, Physics of the Earth and Planetary Interiors 46 (1987) 184–196.
[31] J.B. O'Donovan, W. O'Reilly, Range of non-stoichiometry and characteristic properties of the products of laboratory maghemitization, Earth and Planetary Science Letters 34 (1977) 291–299.
[32] P. Rochette, M. Jackson, C. Aubourg, Rock magnetism and the interpretation of anisotropy of magnetic susceptibility, Reviews of Geophysics 30 (3) (1992) 209–226.
[33] P. Vlag, P. Rochette, M.J. Dekkers, Some additional hysteresis parameters for a natural (titano)magnetite with known grain size, Geophysical Research Letters 23 (20) (1996) 2803–2806.
[34] R.L. Hartstra, Grain-size dependence of initial susceptibility and saturation magnetization-related parameters of four natural magnetites in the PSD-MD range, Geophysical Journal of the Royal Astronomical Society 71 (1982) 477–495.
[35] T. Nishitani, M. Kono, Effect of low-temperature oxidation on the remanence properties of titanomagnetites, Journal of Geomagnetism and Geoelectricity 41 (1989) 19–38.
[36] P. Rochette, G. Lamarche, Evolution des propriétés magnétique lors de transformations minérales dans les roches: exemples du Jurassique Dauphinois (Alpes françaises), Bulletin de Minéralogie 109 (1986) 687–696.
[37] W. Xu, D.R. Peacor, W.A. Dollase, R. van der Voo, R. Beaubouef, Transformation of titanomagnetite to titanomaghemite: a slow, two-step, oxidation-ordering process in MORB, American Mineralogist 82 (1997) 1101–1110.
[38] W. Goetz, P. Bertelsen, C.S. Binau, H.P. Gunnlaugsson, S.F. Hviid, K.M. Kinch, D.E. Madsen, M.B. Madsen, M. Olsen, R. Gellert, G. Klingelhöfer, D.W. Ming, R.V. Morris, R. Rieder, D.S. Rodionov, P.A. de Souza Jr., C. Schröder, S.W. Squyres, T. Wdowiak, A. Yen, Indication of drier periods on Mars from the chemistry and mineralogy of atmospheric dust, Nature 436 (2005) 62–65.
[39] S.F. Hviid, M.B. Madsen, H.P. Gunnlaugsson, W. Goetz, J.M. Knudsen, R.B. Hargraves, P. Smith, D. Britt, A.R. Dinesen, C.T. Mogensen, M. Olsen, C.T. Pedersen, L. Vistisen, Magnetic properties experiments on the Mars Pathfinder Lander: preliminary results, Science 278 (1997) 1768–1770.
[40] R.V. Morris, D.C. Golden, T.D. Shelfer, H.V. Lauer Jr., Lepidocrocite to maghemite to hematite: a pathway to magnetic and hematitic Martian soil, Meteoritics and Planetary Science 33 (1998) 743–751.
[41] V. Barron, J. Torrent, Evidence for a simple pathway to maghemite in Earth and Mars soils, Geochimica et Cosmochimica Acta 66 (15) (2002) 2801–2806.
[42] J. Posey-Dowty, B. Moskowitz, D. Crerar, R. Hargraves, L. Tanenbaum, E. Dowty, Iron oxide and hydroxide precipitation from ferrous solutions and its relevance to Martian surface mineralogy, Icarus 66 (1986) 105–116.
[43] R.G. Burns, Does feroxyhyte occur on the surface of Mars? Nature 285 (1980) 647.
[44] J.E.M. Allan, J.M.D. Coey, M. Resende, J.D. Fabris, Magnetic properties of iron-rich oxisols, Physics and Chemistry of Minerals 15 (1988) 470–475.
[45] H.P. Gunnlaugsson, G. Weyer, Ö. Helgason, Titanomaghemite in Icelandic basalt: possible clues for the strongly magnetic phase in Martian soil and dust, Planetary and Space Science 50 (2002) 157–161.
[46] M.B. Madsen, D.P. Agerkvist, H.P. Gunnlaugson, S.F. Hviid, J. M. Knudsen, L. Vistisen, Titanium and the magnetic phase of Mars, Hyperfine Interactions 95 (1995) 291–304.
[47] P. Rochette, J.-P. Lorand, G. Fillion, V. Sautter, Pyrrhotite and the remanent magnetization of SNC meteorites: a changing perspective on Martian magnetism, Earth and Planetary Science Letters (2001) 1–12.
[48] R.B. Hargraves, J.M. Knudsen, P. Bertelsen, W. Goetz, H.P. Gunnlaugsson, S.F. Hviid, M.B. Madsen, M. Olsen, Magnetic enhancement on the surface of Mars? Journal of Geophysical Research 105 (E1) (2000) 1819–1827.
[49] R.V. Morris, D.C. Golden, J.F. Bell III, H.V. Lauer Jr., Hematite, pyroxene, and phyllosilicates on Mars: implications from oxidized impact melt rocks from Manicouagan Crater, Quebec, Canada, Journal of Geophysical Research 100 (E3) (1995) 5319–5328.
[50] U. Schwertmann, The effect of pedogenic environment on iron oxide minerals, Advances in Soil Science 1 (1985) 171–200.
[51] J.L. Bekley, M.J. Drake, Weathering of Mars–Antarctic analog studies, Icarus 45 (1981) 231–249.
[52] D.T.F. Möhlmann, Water in the upper Martian surface at mid- and low-latitudes: presence, state, and consequences, Icarus 168 (2) (2004) 318–323.
[53] K. Biemann, J. Oro, P. Toulmin III, L.E. Orgel, A.O. Nier, D.M. Anderson, P.G. Simmonds, D. Flory, A.V. Diaz, D.R. Rushneck, J.A. Biller, Search for organic and volatile inorganic compounds in two surface samples from the Chryse Planitia region of Mars, Science 194 (4260) (1976) 72–76.
[54] C.N. Foley, T. Economou, R.N. Clayton, Final chemical results from the Mars Pathfinder alpha proton X-ray spectrometer, Journal of Geophysical Research 108 (E12) (2003) #8096.
[55] J.M. Schäfer, S. Ivy-Ochs, R. Wieler, I. Leya, H. Baur, G.H. Denton, C. Schlüchter, Cosmogenic noble gas studies in the oldest landscape on earth: surface exposure ages of the Dry Valleys, Antarctica, Earth and Planetary Science Letters 167 (1999) 215–226.
[56] G.S. Wilson, J.A. Barron, A.C. Ashworth, R.A. Askin, J.A. Carter, M.G. Curren, D.H. Dalhuisen, E.I. Friedmann, D.G. Fyodorov-Davidov, D.A. Gilichinsky, M.A. Harper, D.M. Harwood, J.F. Hiemstra, T.R. Janecek, K.J. Licht, V.E. Ostroumov, R.D. Powell, E.M. Rivkina, S.A. Rose, A.P. Stroeven, P. Stroeven, J.J.M.V.d. Meer, M.C. Wizevich, The Mount Feather diamicton of the Sirius Group: an accumulation of indicators of Neogene Antarctic glacial and climatic history, Paleogeography, Paleoclimatology, Paleoecology 182 (2002) 117–131.